http://dx.doi.org/10.21611/qirt.2012.166

QIRT 2012

11th International Conference on
Quantitative InfraRed Thermography

InfraRed Image Correlation: a new method for characterizing thermal and displacement fields

by A. Maynadier*, M. Poncelet*, K. Lavernhe-Taillard* and S. Roux*

*Laboratoire de Mécanique et Technologie (LMT Cachan), ENS de Cachan/CNRS UMR 8535/Univ Paris 6/PRES UniverSud Paris, 61 Avenue du Président Wilson, 94230 CACHAN, France, *poncelet @lmt.ens-cachan.fr*

Abstract

Full field measurements, besides its obvious advantage in providing a large amount of information, is crucial for the study of localised phenomena. In order to study thermo-mechanical coupling, this communication presents a new method to jointly measure both thermal and kinematic fields based on images captured with a single infrared camera. It is an enriched global Digital Image Correlation method, where the variations of the optical flow due to the local displacement and to the temperature changes are jointly determined, using a decomposition over a finite element mesh. Here the method is applied to a tensile test on a Shape Memory Alloy and is shown to resolve transformation bands which are only a few pixel wide, and follow their temporal development.

1. Introduction

The characterization of thermodynamically coupled phenomena calls for the measurement of both kinematic and thermal fields. However, obtaining these fields experimentally is difficult as it usually requires two cameras, a (visible light one and an infrared light one) and contradictory coating properties (texture with maximum contrast for full-field kinematic measurement, high and uniform emissivity of the surface for thermography). The operator is often forced to perform these acquisitions on two opposite surfaces for a thin planar sample [1]. An other way to circumvent these problems [2] is to work on specimen preparation to perform temperature and displacement measurement on the same face, still with two different imaging devices. In both cases, a quantitative comparison of the fields in post-processing is tedious if not challenging because the different spatial and temporal discretizations of the two cameras.

A method of image correlation based on a single set of infrared images (InfraRed Image Correlation : IRIC) has been recently developed [4], that evaluates the two types of fields. The proposed method philosophy is to:

(1) Use a textured coating appropriate for DIC algorithm, and get down to the not-so-straight measurement of the temperature with this coating. This means that a thermal “calibration” has to be developed, i.e. one has to find the relationship between the grey level of a pixel, and its true temperature.

(2) Jointly performed the kinematic and thermal measurement. That means extent a DIC algorithm to take into account the grey level variation due to the temperature, that is traditionally supposed constant (optical flow conservation assumption). This way, the same spatial and temporal discretization will be used for kinematic and thermal field (single finite element mesh). Moreover both fields will be intrinsically compensated from each other influence on the IR measure (spurious variation of emissivity due to the displacement of the texture, as well as variation of grey level due to the temperature variation).

(3) Design a relevant coating to ensure both measurements: the texture will consist in black dots of high emissivity paint sprayed over a low emissivity polish metal. The metal will reflect the radiation of the surrounding which is set to a constant temperature, lower than the specimen (figure 1). The coating has enough contrast for DIC and the variation of grey level is linked to the displacement of the specimen or its temperature variation, and nothing else.

In this QIRT communication, the method principles are first presented from the modelling of the grey level evolution to the numerical algorithm and the obtained measurement uncertainties. Then, an application a Ni-Ti SMA specimen submitted to a tension loading, well known for highly coupled kinematics and thermal localisations, due to phase transformation, will be shown.

http://dx.doi.org/10.21611/qirt.2012.166

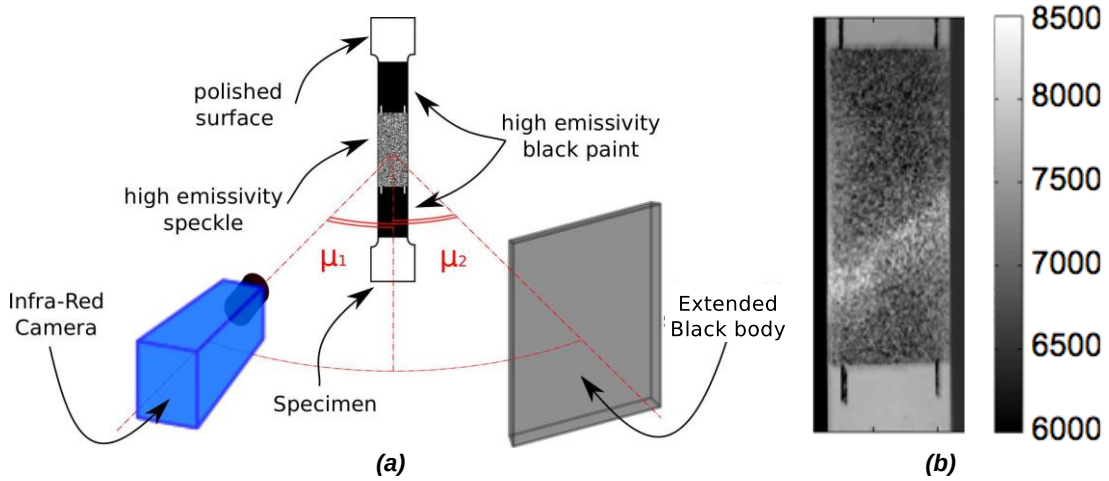

Fig. 1. (a) *Experimental set-up showing the relative position of the IR camera, the specimen surface and the extended black body.* ***(b)*** *Infrared raw picture observed during a tensile test on a Ni-Ti, the color map is given in Digital Level (from 0 to 16000 DL).*

2. IR Image Correlation principle

There are three steps from the camera data to the true temperature (in °C) : the standard camera calibration (to obtain a true temperature in the case of "uniform" sensor, coating and temperature), the link between the apparent temperature (local average grey level) of the speckle and the true temperature (because the average emissivity of the speckle is not equal to one), and the modelling of the link between the local grey level of the speckle to its apparent temperature. These three steps are presented backward to start with the one specific to the presented method. Then the difference of mathematical formulation with a standard global DIC method will be shown in subsection 2.4, and last an uncertainty study is briefly presented (2.5).

2.1. Evolution of the grey level with apparent temperature

First, one has to understand the evolution of the measured grey level with the temperature of the specimen. To do so, one heats it as uniformly as possible with convective heaters up to the maximum temperature it will reach during the test. Its natural cooling is then recorded. The study of the grey level evolution is done with a small area (10 × 10 pixels *i.e.* 2.1 × 2.1 mm^2) to ensure a uniform true temperature.

Figure 2(a) shows the cooling of the small area in the sense of the « apparent temperature » Θ, i.e. mean numerical grey level of the IR camera. One recognizes the usual exponential decrease. Figure 2(b) plots the evolution of the grey level of each pixel with the apparent temperature during the cooling. For each pixel the variation follows a linear relationship, which can be written

$$f(x,t) = a\Theta + b \tag{1}$$

A sensible assumption is that *a* and *b* are linked to the local emissivity of the surface. Considering that the final state of the specimen is a reference state, one may interpret the final image $f_0(x)$ of the cooling as an indirect measure of the emissivity. It is then possible to plot the evolution of $a(x)$ and $b(x)$ with $f_0(x)$, *i.e.* the value of *a* and *b* versus f_0 for each considered pixel (figure 2 (c) and (d)). One again find a linear dependence of *a* and *b* on f_0, so that Eq. (1) is rewritten as

$$f(x,t) = (\alpha_1 f_0(x) + \alpha_2)\Theta + (\beta_1 f_0(x) + \beta_2) \quad . \tag{2}$$

By introducing Θ_0 , the apparent temperature of the reference image f_0 , and Θ_x, the temperature inducing the vanishing of the heterogeneity of measured IR flow (*i.e.* when the radiation emitted by the high emissivity areas of the speckle is exactly equal to the surrounding radiation reflected on the low emissivity areas), one conveniently simplifies the previous equation in

$$f(x,t) = \Theta(t) + \frac{\Theta_x - \Theta(t)}{\Theta_x - \Theta_0}(f_0(x) - \Theta_0)\,. \tag{3}$$

This last formulae has the first advantage to more clearly separate heterogeneity and apparent temperature influences, and also to reduce the number of parameter to identify to a single one (Θ_x) since f_0 and Θ_0 are directly obtained from the IR measurement. One checks that this formulae is appropriate by measuring the difference between left and right members of Eq. (3) during the cooling. At the very beginning of the cooling, Eq. 3 is not exactly verified, but the rest of the evolution is in good agreement with the experimental data. It has been later proved that this was due to the thermal expansion that prevent from an exact still specimen at the beginning.

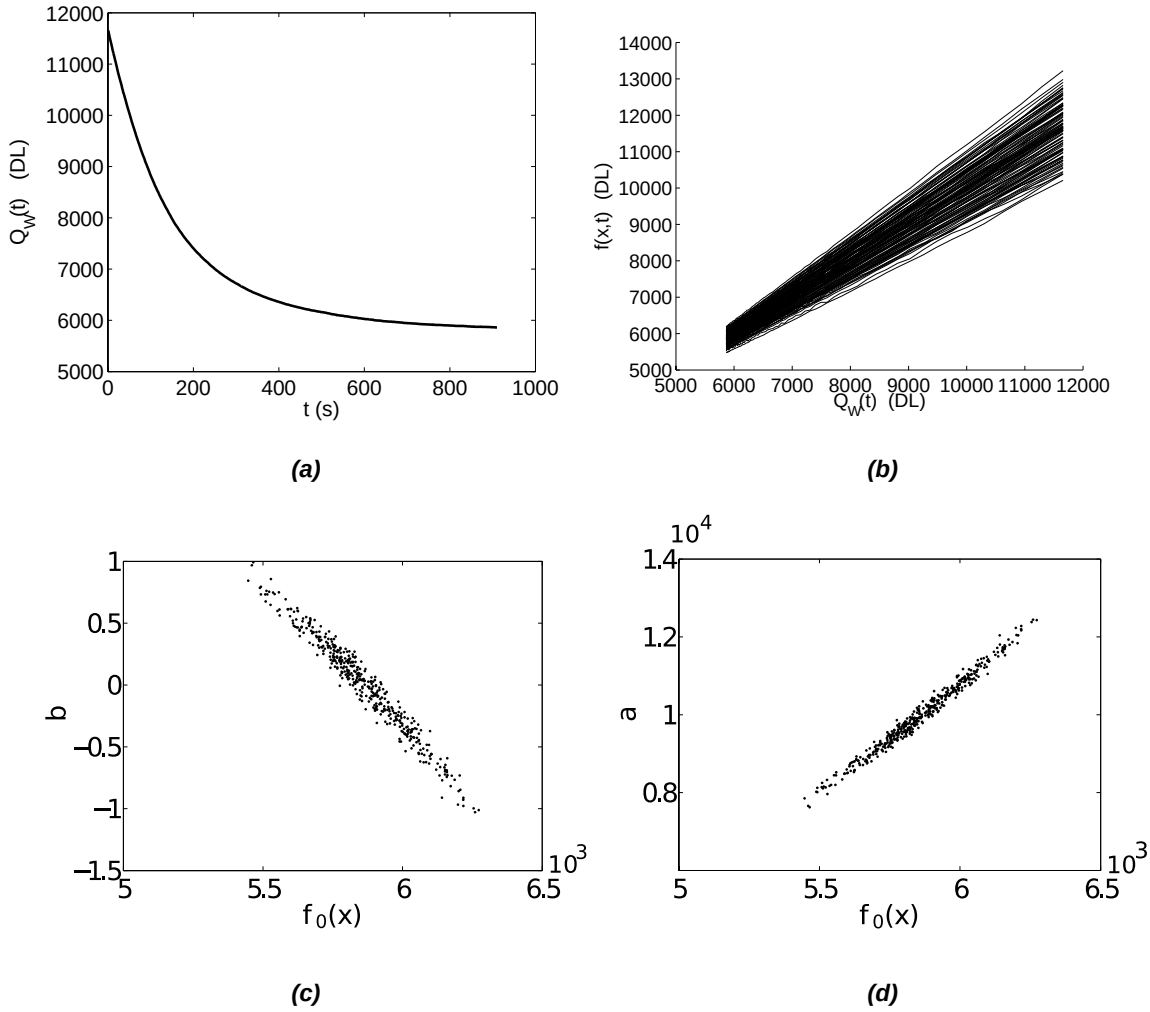

Fig. 2. *Apparent temperature evolution Θ of the small area as a function of time t and (b) grey level evolution of some pixels of the small area as a function of apparent temperature). (c) slope and (d) offset of the grey level dependence on temperature as a function of the reference grey level, $f_0(x)$.*

When one wants to perform this identification on the whole specimen, the assumption of uniform temperature is of course no longer true. One considers that the apparent temperature is described by a low order, *e.g* 4th order polynomial. The identification of Θ_x is now performed with a three-step method. Th first one is the calculation of the guessed temperature from Eq. (3) with an assumed initial value of Θ_x

$$\Theta_{guess} = \frac{\Theta_0(f-\Theta_x)-\Theta_x(f-f_0)}{(f_0-\Theta_x)} \quad . \tag{4}$$

The second step is the fitting of the polynomial on Θ_{guess} to obtain Θ_{smooth} . Last step is the calculation of the new value of Θ_x with Eq. 3 rewritten as

$$\Theta_x = \frac{\langle(\Theta_{smooth}\cdot f_0-\Theta_0\cdot f)(\Theta_{smooth}-\Theta_0+f_0-f)\rangle_{x,t}}{\langle(\Theta_{smooth}-\Theta_0+f_0-f)^2\rangle_{x,t}} \tag{5}$$

where $\langle \ \rangle_{x,t}$ is a spatial and temporal average. One uses an iterative algorithm on Θ_x since the combination of the two previous linear equations and the polynomial fit is a non-linear problem. Convergence is quickly reached (around 8 iterations).

2.2. Evolution of the apparent temperature with the real temperature

This step is very straightforward. To find the relationship between Θ and the true temperature T, the two small black areas at each end of the specimen are exploited. Their coating confers them an emissivity high enough so that they are considered as references from a thermal point of view (T is accurately known there because of the camera own calibration, see section 2.3). One thus has just to tune a multiplicative coefficient so that the extension of the polynomial fit of the apparent temperature Θ is equal to T over these two areas. A typical value of this coefficient is about 1.3, i.e. the average emissivity of the speckle is around 1/1.3~0.75. It is now possible to convert the value of Θ_x (in grey level) into T_x (in Celsius degree). This value is around 8°C in the present experiment, which is in good agreement with the contribution of the black body temperature (4°C) to the temperature of the surrounding.

2.3. Calibration of the camera

The calibration of the camera follows a "standard" one, *e.g.* a 2-point NUC or a pixel-to-pixel method (or so-called "N-NUC") [5] using an extended blackbody, over the whole range of temperature that will be investigated during the experiment.

2.4. Adaptation of a Digital Image Correlation algorithm to IR Image correlation

As stated before, using the algorithm and formulation of the "standard" global DIC [5] allows to jointly solve both kinematic and thermal problems, using the same mesh. For the sake of brevity, here are only underlined the two major modifications to be done to such numerical scheme. For a more detailed description of the IRIC or DIC algorithm, see for example [6] and [5].

First, one has to change the assumption of "brightness conservation" into the new relationship found in subsection 2.1 :

$$g(x+u(x)) = f_0(x) \qquad \text{becomes} \qquad g(x+u(x)) = \Theta(x) + \frac{\Theta_x - \Theta(x)}{\Theta_x - \Theta_0}(f_0(x) - \Theta_0) \tag{6}$$

where $g(x)$ is a second image and $u(x)$ is the sought displacement field. This way, it is possible to determine both the displacement field $u(x)$ and the temperature field $\Theta(x)$ thanks to the minimization of an objective function

$$\mathfrak{R}(u,\Theta) = \int \left(g\big(x+u(x)\big) - f_0(x) - \frac{\Theta(x)-\Theta_0}{\Theta_x-\Theta_0}\big(\Theta_x - f_0(x)\big) \right)^2 dx \quad . \tag{7}$$

In the case of the global DIC algorithm, the displacement field is described in a Finite Element Method framework (a mesh with shape functions on each element). The previous minimization problem is then linearized around a given solution, and solved iteratively. The mesh size is decreased gradually to its prescribed value to ensure a quick and accurate convergence. One interesting point of the proposed approach is that once more the entire algorithm of DIC may be kept, provided a second simple modification. One has to "extend" the original elementary vector used to build the numerical problem. Usually this vector only contains the gradients of the grey level $\partial_1 f_0(x)$ and $\partial_2 f_0(x)$, whereas in the present method it must also contain the information of grey level itself $f_0(x)$. A convenient way to introduce the latter is to add a relative grey level as a third component :

$$G = \begin{pmatrix} \partial_1 f_0(x) \\ \partial_2 f_0(x) \end{pmatrix} \qquad \text{becomes} \qquad G = \begin{pmatrix} \partial_1 f_0(x) \\ \partial_2 f_0(x) \\ \frac{f_0(x)-\Theta_x}{\Theta_0-\Theta_x} \end{pmatrix}. \tag{9}$$

It is thereafter possible to jointly solve both kinematic and thermal field with a single minimization.

2.5. Kinematic and thermal uncertainties

Three analysis campaigns are carried out to assess the displacement, strain and temperature measurement uncertainties. For each quantity, different uniform fields are artificially imposed to the same reference image (the last one from the calibration procedure record) to generate test images. The IRIC algorithm is then applied separately to each of the test images and the reference one. Four mesh sizes are used from 24 × 24 pixels down to 6 × 6 pixels. Two

indicators are used to assess the measurement accuracy: the systematic error (mean error to the prescribed value) and the standard uncertainty (standard deviation of the computed field).

When uniform sub-pixel displacement fields are imposed, one notes that the systematic error is independent of the mesh size, with typical values lower than 5×10^{-2} pixel for 12 × 12 mesh size. As for a ”standard” global DIC algorithm, the uncertainty decrease with the mesh size and is independent of the prescribed displacement (figure 3a). The temperature field is also independent of the displacement, and its standard deviation is less than 5×10^{-2} °C, apart from boundary elements where values are slightly more important.

When uniform strain fields from 10^{-4} to 16×10^{-4} are imposed, the strain is globally overestimated (mean systematic error around 2×10^{-4} for these prescript strains). The systematic error is also slightly dependent on the mesh size, probably because of the strain calculation method. The strain uncertainty is nonetheless appreciable, ranging from 10^{-4} to 10^{-3} for mesh size 12 × 12 (figure 3b). Once more the temperature field is not affected by the prescribed strain. The correlation residual (i.e. the pixel-to-pixel difference between the reference image and the deformed image once corrected by the measured displacement) remains very low, less than 20 grey levels for an original grey level range around 1000).

Last, uniform temperature fields are imposed to the reference image, according to the grey level – temperature relationship given Eq. 3. Figure 3c shows that the temperature uncertainty is only slightly dependent on the mesh size. This uncertainty, due to the algorithm itself, is very low (around 10^{-4} to 10^{-3} ◦C) when compared to the camera own measurement uncertainty (NETD around 2×10^{-2} ◦C in our case). The kinematic fields are not influenced by the prescribed temperature field, as temperature field was not by prescribed kinematic fields.

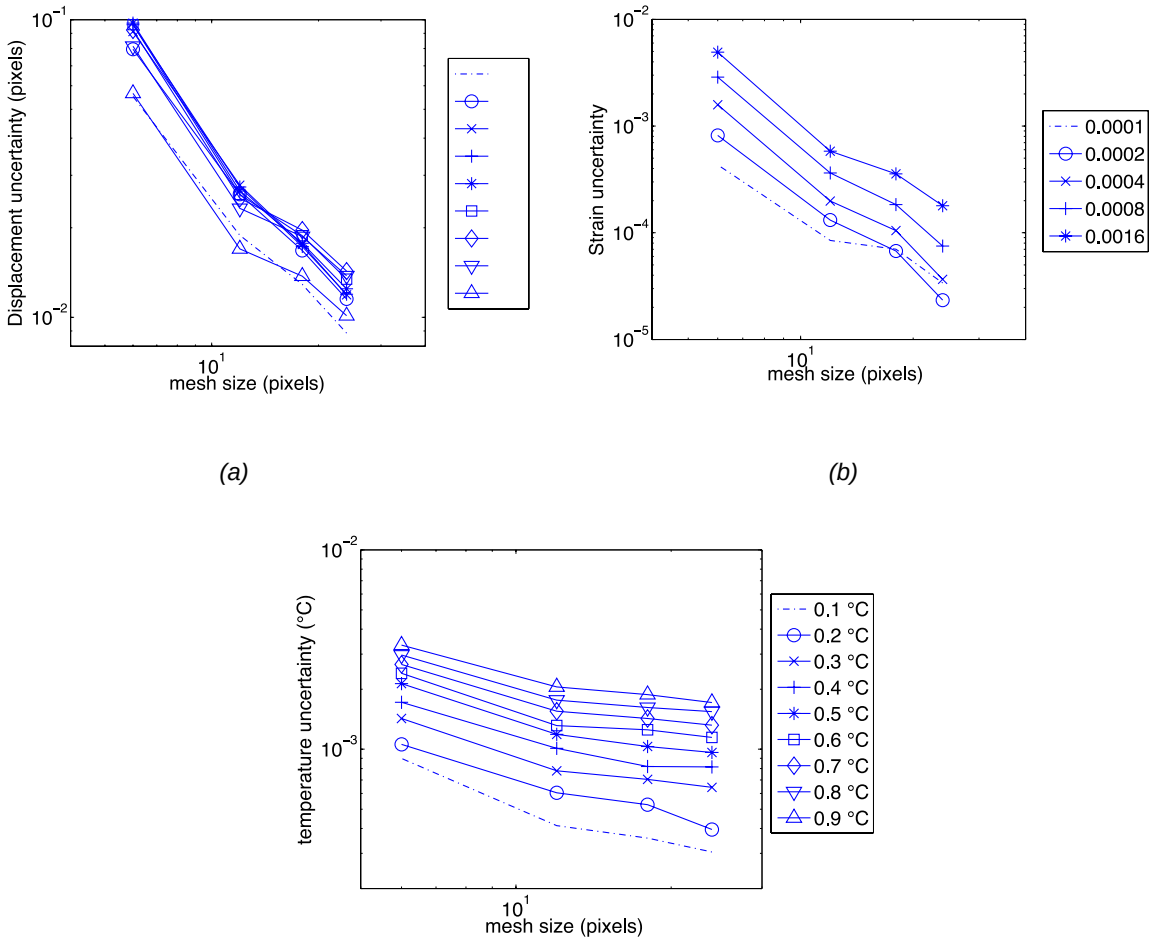

Fig. 3. *Uncertainty results. (a) Displacement uncertainty for an imposed subpixel displacement (0.1 to 0.9 pix.). (b) Strain uncertainty for an imposed strain (10^{-4} to 16×10^{-4}). (c) Temperature uncertainty for an imposed temperature (0.1 to 0.9 °C).*

It is worth noticing that when the same images are processed by the standard DIC software from which IRIC is derived (Correli-Q4 [6]), the displacement uncertainty is only around 2.5 times smaller. Concerning strain uncertainty, both standard uncertainty and systematic error are of the same order of magnitude than IRIC ones. The extra information that is given by IRIC method, i.e. the temperature field, has thus nearly no influence on the quality of the kinematic field. A key point to this feature is the gradual decrease of mesh size in the algorithm, ensuring robustness despite a higher number of degrees of freedom.

3. Application to a SMA specimen

3.1. Experimental set-up

The material used for the test has a $Ni_{49,75\ at\%}Ti$ composition (commercial name SE508). Their forming consists mainly in a cold-rolling, followed by a heat treatment of 2 minutes at 480°C in a salt bath. Samples are flat bone shaped, their cutting performed by electro-erosion and followed by electro-chemical polishing. They have a rectangular section of 20 × 2 mm^2 and a gauge zone length of 120 mm. The transformation temperatures have been estimated thanks to Differential Scanning Calorimetry (DSC) measurement. Only two phase changes are visible so the rhombohedral phase (R-phase) is assumed to not occur for this specific forming and heat treatment. The determined transition limits are: austenite start As = 13 °C, austenite finish Af = 23 °C, martensite start Ms = 21 °C and martensite finish Mf = 8 °C. The thermal experimental conditions ensure a full austenite material at the beginning of the mechanical test.

A high emissivity (0.95) paint is sprayed on the surface of interest, originally of low emissivity (0.2) to produce a random speckle pattern of highly contrasted emissivity. The high emissivity coating uniformly covers the two ends of the specimen. The specimen is then put in the experimental set-up as schematically shown figure 1. Typical distances between specimen and camera, and specimen and black body are equal, about 30 cm. The testing machine is a 100 kN hydraulic MTS machine. The IR camera is a Cedip Jade III recording at 100 Hz with a 50 mm fixed lens, so that the physical size of a pixel is about 210 µm. The Integration Time (IT) is set to 930 µs to avoid saturation of sensors when the specimen temperature reaches its climax. The experimental workspace, including imaging devices, is isolated from the surrounding in order to keep the thermal and ventilation condition as constant as possible. The ambient temperature is around 27.5 °C and the black body temperature set to 5 °C.

The calibration procedure is then performed. The specimen is heated with convective heaters, and its load-free cooling is recorded with the IR camera. The numerical procedure described in subsection 2.1 is followed to find Θ_x, and the coefficient linking apparent and true temperature is calculated with the help of the to ends of the specimen and the method described in subsection 2.2.

3.2. Results

The curve of figure 4a represents the elongation versus the global stress measured by the machine. The shape is typical of a pseudo elastic behavior, and is roughly interpreted as follow:

- A first linear part (ended around 350MPa and 1.1%) corresponding to the elasticity of the austenite phase.
- A plateau of 4.6%, during which localized austenite to martensite transformation occurs.
- At the end of austenite transformation, a second linear part, with pure elasticity of the martensitic phase.

Theses quantities are directly measured on the testing machine sensors, so that they only provide global and potentially biased measurements.

On the contrary, figure 4b presents the local thermal and kinematic evolutions of three different points during the same test. These results are obtained with IRIC method, but presented as if obtained by single-point sensors, *e.g.* 3 strain gauges and 3 thermocouples. The interpretation is not straightforward to an eye non accustomed to localization phenomena. During step II, a transformation band appears around the 44th second, inducing a strain increase up to 6%, then the band enlarges and the heat is released only ahead of the bands. Though the localization feature of the phenomenon is shown, it is still difficult, if not impossible, to quantify accurately its kinetics.

The full field measurements are presented figure 5 at four different times. From a technical point of view, one notes that despite the rather low resolution of the camera (around 100 pixel along the width of the specimen), the measured field is quite rich. This is because of the well-designed algorithm that enables the use of small mesh sizes (here 12 x 12 pixels) without increasing too much the standard uncertainty. Larger elements smear out the shear band over a larger region, whereas smaller ones display a significant amount of fluctuations. In the present case, the standard strain uncertainty as well as temperature uncertainty is clearly lower than the observed phenomenon.

As far as the material behavior is concerned, they show the systematic simultaneity of strain increase and heat release that is interpreted as a high coupling. Moreover, it allows us to decomposed the NiTi SMA's behaviors in two steps: the uniform one, where the elastic response of the austenite is mixed with the appearance of diffuse martensite, and the localized one, where bands occur and enlarge. The local aspect of the measurements, added to the high temporal discretization allows for the quantitative estimate of the observation of the way of appearance and the propagation celerity of the bands, depending on the loading rate.

http://dx.doi.org/10.21611/qirt.2012.166

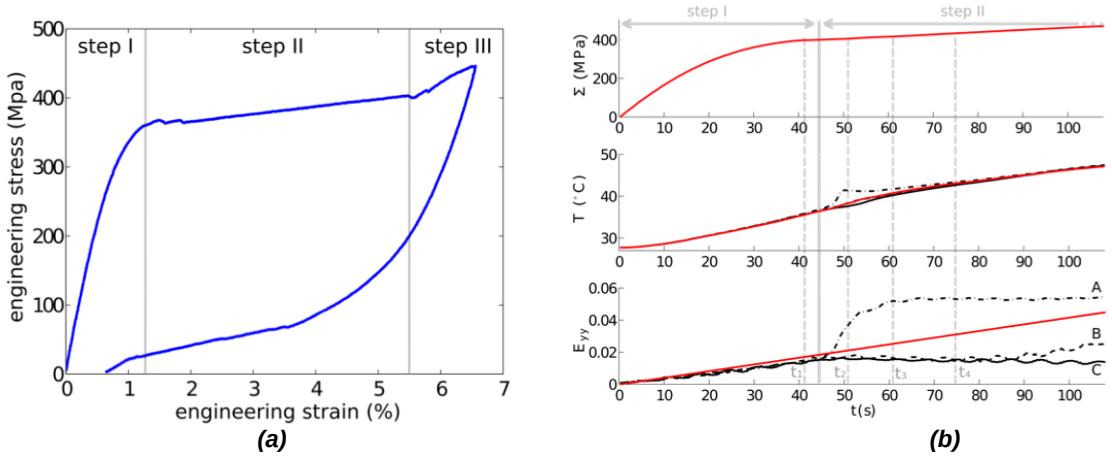

Fig. 4. *Comparison between global and local measurements. (a) Experimental tensile curve at 0.01 mm.s^{-1}, quantities are engineer ones, measured on the testing machine. (b) Simultaneous evolution of the stress, the temperature and the longitudinal strain. Red lines are macroscopic quantities whereas doted lines are local quantities in three physical points (A,B,C).*

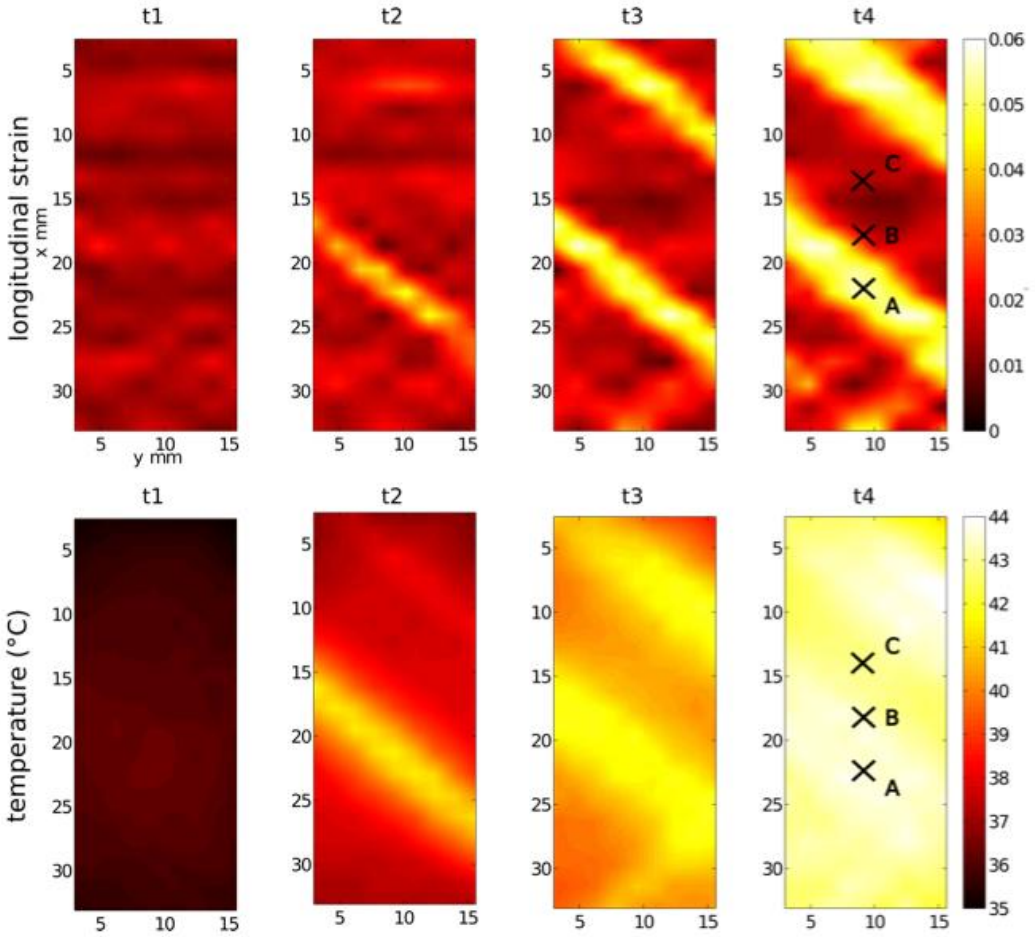

Fig. 5. *Temperature and longitudinal strain fields at four typical instants (t_1 = 42 sec, t_2 = 51,25 sec, t_3 = 61,25 sec, t_4 = 75 sec)*

4. Conclusions

The method presented in this communication was mainly developed to get round the post-synchronization and association steps of the kinematic and thermal field obtained with usual two-camera setups. It has the secondary advantage to clearly take into account the coating heterogeneous emissivity, instead of trying to find a uniform one, or neglect its heterogeneity. A third pro of this method is that it requires a single camera (no distortion correction, no synchronization problems).

The key point of the method is to change the brightness conservation assumption of a standard DIC algorithm to another law were the evolution of the brightness is related to the evolution of the local temperature. One expects this law to be complicated, but it turns out to be a simple linear relationship once expressed with the appropriate parameter, namely the vanishing temperature Θ_x.

The standard global DIC algorithm has of course to be changed, but the modifications result in the simple exchange of the standard elementary vector containing the grey level gradients of the image by a vector containing the gradients and the grey level itself. The displacement and temperature fields are still decomposed onto a basis of continuous functions as proposed in finite element methods. Kinematic and thermal fields are jointly determined through a single minimization.

One could fear that the addition of the thermal unknowns to the standard DIC problem may deteriorate the convergence of the algorithm and increase the uncertainty of the results. Nonetheless, the uncertainty analysis proves that the algorithm, containing a gradual decrease of the mesh size, is robust and gives kinematic uncertainties that are only a little bit higher that the ones of standard global DIC. The “extra” field provided by the method (the temperature) has also a very low standard uncertainty, below the NETD of today high-end IR cameras. Of course some improvements can still be made. As an example, the weak spatial resolution of the images provided by IR cameras could be compensated by the high acquisition rate available by using an adequate spatio-temporal correlation [7].

Last, when applied to a NiTi Shape Memory Alloy under tension, this method enables the measurement of both the thermal and kinematic features of the martensitic transformation bands. This proves that this technique is fully operable, and of interest, in the case of such localized phenomena.

REFERENCES

[1] Chrysochoos A., Berthel B., Latourte F., Galtier G., Pagano S., Wattrisse B., *Local energy analysis of high-cycle fatigue using digital image correlation and infrared thermography*, Journal of Strain Analysis for Engineering Design, vol. 43, pp. 411-421, 2008.

[2] Schlosser P.,Louche H., Favier D. Orgéas L. “Thermomechanical observation of phase transformation during tensile test on Ni-Ti tubes.” Strain, vol. 43, pp. 260-271, 2007.

[3] Bodelot L., Sabatier L., Charkaluk E., Dufrénoy P., "Experimental setup for fully coupled kinematic and thermal measurements at the microstructure scale of an AISI 316L steel" Material Science Engineering vol. A 501, pp. 52-60, 2006.

[4] Maynadier A., Poncelet M., Lavernhe-Taillard K. and Roux S., “One-shot measurement of thermal *and* kinematic fields : InfraRed Images Correlation” Experimental Mechanics vol. 52 pp. 241-255, 2012.

[5] Schulz M., Caldwell L., *Nonuniformity correction and correctability of infrared focal plane arrays*, Infrared Phys. Technol. vol 36 pp. 763-777, 1995.

[6] Besnard G., Hild F., Roux S. "Finite element displacement fields analysis from digital analysis: application to Portevin-le Châtelier Bands”. Experimental Mechanics, vol. 46, pp. 789-803, 2006.

[7] Besnard G., Leclerc H., Hild F., Roux S., Swiergiel N., “Analysis of image series through global Digital Image Correlation”, to appear in J. Strain Analysis.